Instability analysis of pressurized pipes with longitudinal surface cracks

Diya Arafah [a], Mauro Madia [b,*], Uwe Zerbst [b], Stefano Beretta [a], Mihaela Eliza Cristea [c]

[a] Politecnico di Milano, Department of Mechanical Engineering, I-20156 Milano, Italy
[b] BAM Federal Institute for Materials Research and Testing, Division 9.1, D-12205 Berlin, Germany
[c] Tenaris Dalmine, R&D, Piazza Caduti 6 Luglio 1944, I-24044 Dalmine, Italy

Received 12 March 2014 Received in revised form 8 January 2015
Accepted 9 January 2015 Available online 19 January 2015

1. Introduction

The structural assessment of pressurized components is an important issue in many engineering applications, e.g., in the nuclear and oil & gas industry, where the risk of component failure must be minimized because of severe failure consequences [1]. In case of steel components, surface defects (corrosion pits, dents) are the most common flaws at which fatigue cracks develop. These must be considered in component assessment, as their propagation could finally lead to failure [2]. Besides theoretical analyses it is important to perform experimental tests in order to assess the load-carrying capacity of the cracked components. In the case of pressurized components burst tests are carried out in order to evaluate the critical pressure [3].

Common flaw assessment methods [4,5] require the accurate determination of the material fracture resistance. This can be measured following standard test procedures [6] which make use of specimens that are highly constrained to plastic deformation in order to provide lower bound estimates of the fracture resistance.

* Corresponding author. Tel.: +49 30 8104 4166; fax: +49 30 8104 1539.
E-mail address: mauro.madia@bam.de (M. Madia).

For elastic–plastic failure analyses, besides the stress intensity factors, limit load solutions of cracked components are needed, which can be found in handbooks [7,8]. These solutions were obtained for different yielding conditions and their accuracy is usually not well known. In order to improve the accuracy, new solutions have been generated based on finite element analyses during the last years. In particular, recent solutions for surface and through-thickness cracks in cylinders under internal pressure are provided in Refs. [9–11].

In Refs. [12,13] three of the authors of the present paper presented analytical parametric solutions for what they call reference loads for tension, bending, combined tension-bending and biaxial tension loading of plates with semi-elliptical surface cracks (see also Ref. [14]). Solutions have been also provided based on stresses, defining what the authors call reference yield stress σ_0. It must be remarked that the reference load is not a limit load, but it is rather an alternative to the limit load and it has been developed in order to obtain a better description of the crack driving force as a function of the applied load. The approach allows a wider application range and the solutions demonstrated to provide more accurate crack driving force estimates compared with the ones based on common limit load solutions, especially in case of large cracks [13]. A brief summary of the basics of the reference load,

Nomenclature

a	crack depth (Fig. 1)
a_0	initial crack depth assumed or existent in the component
a_c	critical crack depth at failure
c	crack semi-length (Fig. 1)
c_0	initial crack semi-length assumed or existent in the component
c_c	critical crack semi-length
$f(L_r)$	ligament yielding correction function (Eqn. (12))
l	length of the pipe
p	internal pressure
p_c	critical internal pressure, failure pressure
w_j	coefficients of the weight function (Eqn. (2))
A	deepest point of the crack front (semi-elliptical surface cracks)
B	specimen thickness
B_N	specimen net thickness
C	surface points of the crack front (semi-elliptical surface cracks)
C_i,C_{ii}	fitting parameters in the reference yield stress solutions (Eqns. (3)–(5), (7), (8), (14)–(17))
CDF	crack driving force
CMOD	crack mouth opening displacement (R-curve testing)
D_o	nominal outer diameter of the pipe
E	modulus of elasticity
EDM	electric discharge machining
E'	effective modulus of elasticity (E for plane stress; $E/(1-\nu^2)$ for plane strain)
FAD	failure assessment diagram
F_0	reference load
H	distance between grips (Fig. 6)
J	integral
J_e	elastic J-integral (K^2/E')
K	stress intensity factor, K-factor
L_r	ligament yielding parameter (Eqn. (11))
$L_r^{\max}$	localized plastic collapse limit (Eqn. (13))
R-curve	crack resistance curve, in the present paper given as $J-\Delta a$ curve
R_m	ultimate tensile strength
SIF	stress intensity factor
T	wall thickness of the pipe and of plates
W	specimen width (Fig. 6)
α	correction factor for the bending stress component (Eqn. (22))
ε	strain (general notation)
ε_{ref}	reference strain (Eqn. (12))
γ	proportionality factor between bending and membrane stress
λ	biaxial stress ratio (Eqn. (6))
ν	Poisson's ratio
σ	stress (general notation)
σ_a	axial stress (Eqn. (23))
σ_{app}	applied stress
σ_b	bending stress
$\sigma_{b,0}$	reference bending yield stress under pure bending (Eqn. (17))
$\sigma_{biax,0}$	reference yield stress under biaxial tensile loading (Eqn. (5))
σ_j	stress coefficients (Eqn. (1) and Eqn. (2))
σ_{ref}	reference stress (Eqn. (12))
σ_m	membrane stress
σ_m^*	reduced reference tensile yield stress under combined loading (Fig. 3)
σ_0	reference yield stress, general notation (Eqn. (11))
$\sigma_{m,0}$	reference yield stress for tensile loading (Eqn. (3))
σ_x	remote stress in x direction (Fig. 1)
σ_r	radial stress (Eqn. (23))
σ_θ	hoop stress (Eqn. (23))
σ_y	remote stress in y direction (Fig. 1)
σ_Y	yield strength (general), either R_{eL} or $R_{p0.2}$
ξ	coordinate through the wall thickness (Eqns. (1) and (2)), general notation
Δa	stable crack extension

respectively reference yield stress, approach is provided in the Appendix.

Within this study the reference yield stress solutions for plates under biaxial tensile loading have been applied to the assessment of thick-walled pressurized pipes and validated against four burst tests. The use of substitute geometries (plates) for the structural integrity assessment of these pipes was discussed by some of the authors in previous works, in which J-integral analytical estimates for plates were compared to the values calculated by means of finite element simulations on pipes [15,16].

Axial semi-elliptical surface cracks of different size were introduced on the outer surface of the pipe by electric discharge machining (EDM) and subsequent cyclic loading. Component analysis has been conducted analytically, thus giving a straightforward approach and time efficient tool compared to other methods (e.g. finite elements). The analytical procedure demonstrated to yield good predictions (slightly conservative) of the burst pressures.

2. The fracture mechanics approach

2.1. The proposed methodology

In the present study a methodology is developed for predicting the instability of pressurized pipes subjected to complex loading conditions different from uniaxial loading. The principle follows methods such as R6 [4] or SINTAP/FITNET [5]. The stress profile (assumed as two dimensional) is determined for the component without crack. This can be done by finite elements or, as in the present case, analytically. It is then applied to a substitute geometry (a plate or a hollow cylinder) depending on the component to be investigated. Based on the stress profile, which is usually fitted by a polynomial, the K-factor and the limit load or, as proposed by the authors, the reference load is determined for the deepest and the surface points of the crack (points A and C respectively).

The proposed method consists of a number of subsequent steps that will be explained in this section.

2.1.1. Step 1: determination of the stress profile in the component without crack

The stress profiles can be obtained by finite elements or by analytical methods, however, all loading components have to be considered. In the general case this may include the applied service loads such as external forces, moments or pressure, dead weight and inertia loads, thermal stresses, residual stresses (welding residual stresses, press fit stresses, etc.), and stresses due to mechanical resonance. For pressurized components it is important to consider biaxial tension loading as presented in Ref. [15] and in the validation example in this paper.

2.1.2. Step 2: determination of the stress intensity factor (K-factor)

The determination of the stress intensity factor for mode I loading is usually based on the stress profile obtained in step 1 which is then approximated by a polynomial

$$\sigma(\xi,T)=\sum_{j=0}^{n}\sigma_j\cdot\left(\frac{\xi}{T}\right)^j=\sigma_0+\sigma_1\cdot\left(\frac{\xi}{T}\right)+\sigma_2\cdot\left(\frac{\xi}{T}\right)^2+\ldots+\sigma_n\cdot\left(\frac{\xi}{T}\right)^n \tag{1}$$

where n is the order of the polynomial (in common practice third- to sixth-order polynomial are used in conjunction with weight function solutions to determine the K-factor), T is the wall thickness, and ξ is the distance from the surface through the wall thickness. The hoop stress σ_θ has been used for the calculation of the K-factors, being the stress perpendicular to the crack plane in the case of axial flaws, as investigated in this work. The polynomial coefficients σ_j are then applied in conjunction with a weight function solution, the general form of which is

$$\begin{aligned}K&=\sum_{j=0}^{n}\sigma_j\cdot w_j\cdot\left(\frac{a}{T}\right)^j\cdot\sqrt{\pi\cdot a}\\&=\left[\sigma_0\cdot w_0+\sigma_1\cdot w_1\cdot\left(\frac{a}{T}\right)+\sigma_2\cdot w_2\cdot\left(\frac{a}{T}\right)^2+\ldots+\sigma_n\cdot w_n\cdot\left(\frac{a}{T}\right)^n\right]\cdot\sqrt{\pi\cdot a}\end{aligned} \tag{2}$$

Note that the different terms in the bracket refer to different stress components due to different loading (e.g., σ_0 is a membrane stress, σ_1 a bending stress and the higher coefficients from σ_2 upwards may represent a notch stress). Solutions for given geometrical configurations and load cases are provided in compendia of flaw assessment methods, such as R6 [4], or in specific handbooks [17]. A more comprehensive overview on this topic is provided in Ref. [5]. In the validation example of the present study, the K-factor solution for semi-elliptical surface cracks in pipes according to Newman–Raju [18] has been applied.

2.1.3. Step 3: determination of the reference yield stress for uniaxial tension neglecting the bending stress component

In this step the reference yield stress (cf. Appendix) is calculated considering uniaxial tension stresses acting normal to the crack plane. Both the bending stress component in the combined loading (see step 6) and the biaxial stress parallel to crack (see step 4) are neglected in this step. The reference yield stress under pure tension $\sigma_{m,0}$ is provided in Ref. [13] and determined by:

$$\sigma_{m,0}=\left\{C_0+C_1\cdot\left[\frac{a\cdot c}{T\cdot(T+c)}\right]+C_2\cdot\left[\frac{a\cdot c}{T\cdot(T+c)}\right]^2\right\}\cdot\sigma_Y \tag{3}$$

$$\text{with } C_0=\min\begin{cases}C_{00}+\dfrac{\sigma_Y}{C_{01}}\\1\end{cases} \tag{4}$$

The coefficients C are provided in Table 1, where the indices A and C refer to the deepest and the surface points of the crack respectively.

Table 1
Coefficients C in Eqns. (3) and (4).

Point at crack front	C_{00} [−]	C_{01} [MPa]	C_1 [−]	C_2 [−]
A	0.9245	5419	−0.5297	0.3863
C	0.9491	5863	−0.3050	−0.5000

2.1.4. Step 4: correction of the uniaxial reference yield stress for biaxial tension loading

In this step the biaxial stress acting parallel to the crack will be considered by using a correction function applied to the uniaxial reference yield stress $\sigma_{m,0}$ calculated in step 3 as follows:

$$\frac{\sigma_{biax,0}}{\sigma_{m,0}}=C_0(\lambda)+C_1(\lambda)\cdot\left[\frac{a\cdot c}{T\cdot(T+c)}\right]+C_2(\lambda)\cdot\left[\frac{a\cdot c}{T\cdot(T+c)}\right]^2 \tag{5}$$

with λ being the biaxial stress ratio defined as the ratio of the stresses in x and y-direction (see Fig. 1)

$$\lambda=\sigma_x/\sigma_y. \tag{6}$$

The coefficients C are

$$\text{Point A}\begin{cases}C_0(\lambda)=1+0.0348\cdot\lambda+0.0293\cdot\lambda^2\\C_1(\lambda)=0.4176\cdot\lambda+0.1751\cdot\lambda^2\\C_2(\lambda)=-1.8381\cdot\lambda+0.7952\cdot\lambda^2\end{cases} \tag{7}$$

$$\text{Point C}\begin{cases}C_0(\lambda)=1-0.1311\cdot\lambda+0.1271\cdot\lambda^2\\C_1(\lambda)=0.4638\cdot\lambda-0.0551\cdot\lambda^2\\C_2(\lambda)=-1.5114\cdot\lambda+1.1020\cdot\lambda\end{cases} \tag{8}$$

when using the equivalent von Mises stress in the definition of the reference yield stress under biaxial tensile loading [13]. After the reference yield stress under biaxial loading $\sigma_{biax,0}$ has been determined, the fracture assessment can be conducted in the next step.

2.1.5. Step 5: determination of the critical loads and critical crack dimensions

The fracture instability analysis is done using tearing instability or R-curve methodology [5]. The J-integral as the crack driving force parameter for elastic–plastic deformation behavior is obtained using the R6 method or SINTAP/FITNET as

$$J=J_e\cdot[f(L_r)]^{-2} \tag{9}$$

The elastic J-integral J_e is calculated from the stress intensity factor (K-factor) obtained in step 2 as

$$J_e=K^2/E\prime \tag{10}$$

with $E'=E$ for plane stress and $E'=E/(1-\nu^2)$ for plane strain assumption. Usually the plane stress assumption is preferred in flaw assessment to ensure conservatism. The term $f(L_r)$ is a ligament plasticity correction function expressed in terms of the ligament yielding parameter L_r. In Ref. [13] the authors propose a generalized formulation of the ligament yielding parameter L_r as:

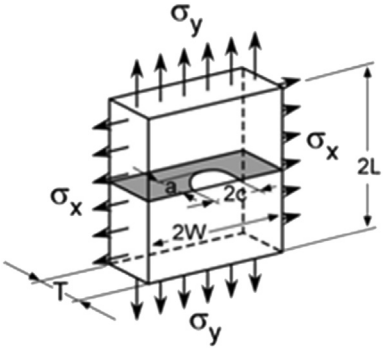

Fig. 1. Biaxial loading of a plate with a semi-elliptical surface crack.

$$L_r = \sigma_{app}/\sigma_0 \tag{11}$$

where σ_{app} is the applied stress and σ_0 the reference yield stress. The $f(L_r)$ function can be determined for different conservative analysis options in assessment methods such as R6 (see Ref. [5]). The best results are obtained by the Option 2 which uses the complete true stress–strain curve of the material, which writes:

$$f(L_r) = \left[\frac{E\cdot\varepsilon_{ref}}{\sigma_{ref}} + \frac{1}{2}\cdot\frac{\sigma_{ref}}{E\cdot\varepsilon_{ref}}\cdot L_r^2\right]^{-1/2} \tag{12}$$

The reference yield stress σ_0 must not be confused with the reference stress σ_{ref} defined, e.g., in BS 7910 [8], which is fully determined by the component information (geometry and loading). Fig. 2 shows also how the reference strain ε_{ref} in Eqn. (12) is calculated based on the true stress–strain curve. If the stress–-strain curve of the material under investigation is not available, lower analysis options within the R6 or SINTAP procedure can be used to define the plastic correction function $f(L_r)$.

The method described by now refers to tearing instability i.e. unstable crack extension following some stable ductile tearing, however, potential plastic collapse terminating the stable tearing phase has also to be considered as a competing failure mode when the deformation behavior is elastic–plastic. The cut-off to prevent localized plastic collapse is set at the point at which $L_r = L_r^{\max}$, where

$$L_r^{\max} = \frac{1}{2}\cdot\frac{\sigma_Y + R_m}{\sigma_Y}. \tag{13}$$

2.1.6. Step 6: correction for the bending stress component within the combined loading

The combined loading may be described either by the membrane stress component σ_m or the bending stress component σ_b, and similarly, using the corresponding reference yield stresses as normalizing stresses $\sigma_m/\sigma_{m,0}$ and $\sigma_b/\sigma_{b,0}$. In the assessment analysis the membrane stress component is used as the basis for describing the combined loading and the assessment results will subsequently be corrected for the bending stress components using a correction factor α as explained below. A polynomial function had been proposed in Ref. [13] to describe the interaction between membrane and bending stress components for combined loading such as shown in Fig. 3. The abscissa represents the tension stress component while the ordinate represents the bending stress component.

The interaction function is expressed as:

$$\frac{\sigma_b}{\sigma_{b,0}} = 1 + C_1\cdot\left(\frac{\sigma_m}{\sigma_{m,0}}\right) + C_2\cdot\left(\frac{\sigma_m}{\sigma_{m,0}}\right)^2 - (1 + C_1 + C_2)\cdot\left(\frac{\sigma_m}{\sigma_{m,0}}\right)^3 \tag{14}$$

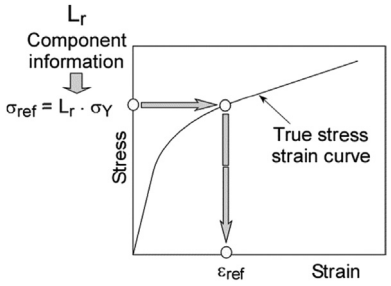

Fig. 2. Definition of reference stress and strain, σ_{ref} and ε_{ref}, on the true stress–strain curve in the Option 2 of R6 procedure.

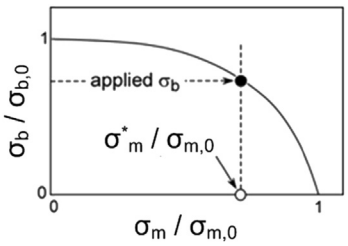

Fig. 3. Combined tension and bending loading.

$$\text{with } C_1 = C_{10} + C_{11}\cdot\left[\frac{a\cdot c}{T\cdot(T+c)}\right] \tag{15}$$

$$\text{and } C_2 = C_{20} + C_{21}\cdot\left[\frac{a\cdot c}{T\cdot(T+c)}\right] \tag{16}$$

The coefficients C are given in Table 2.

In Eqn. (14) $\sigma_{m,0}$ is the reference yield stress under pure tension as calculated in Eqn. (3) and $\sigma_{b,0}$ is the reference yield stress under pure bending [13] which can be calculated by:

$$\sigma_{b,0} = \left\{C_0 + C_1\cdot\left[\frac{a\cdot c}{T\cdot(T+c)}\right]\right\}\cdot\sigma_Y \tag{17}$$

with the coefficients C given in Table 3

The membrane (σ_m) and bending (σ_b) stress components of the stress profile across the wall thickness can be calculated as follows:

$$\sigma_m = \frac{1}{T}\cdot\int_0^T \sigma d\xi \tag{18}$$

$$\sigma_b = \frac{6}{T^2}\cdot\int_0^T \sigma\cdot\left(\frac{T}{2} - \xi\right)d\xi \tag{19}$$

If an approximation of the stress profile is available as a sixth-order polynomial, the series expansion of Eqns. (18) and (19) can be used to determine the stress components as [5]:

$$\sigma_m = \sigma_0 + \frac{1}{2}\cdot\sigma_1 + \frac{1}{3}\cdot\sigma_2 + \frac{1}{4}\cdot\sigma_3 + \frac{1}{5}\cdot\sigma_4 + \frac{1}{6}\cdot\sigma_5 + \frac{1}{7}\cdot\sigma_6. \tag{20}$$

$$\sigma_b = -\frac{1}{2}\cdot\sigma_1 - \frac{1}{2}\cdot\sigma_2 - \frac{9}{20}\cdot\sigma_3 - \frac{2}{5}\cdot\sigma_4 - \frac{5}{14}\cdot\sigma_5 - \frac{9}{28}\cdot\sigma_6 \tag{21}$$

In the case of proportional loading, the ratio between the tension stress σ_m and the bending stress σ_b components will be constant.

The assessment results obtained in step 5 can be corrected for the bending stress component σ_b by reducing the critical stress σ_m to σ_m^*. Similarly, using the normalized notation, $\sigma_m/\sigma_{m,0}$ must be reduced to $\sigma_m^*/\sigma_{m,0}$ such as illustrated in Fig. 3.

The reduction factor can be determined by solving Eqn. (14) iteratively for $\sigma_m^*/\sigma_{m,0}$ with $\sigma_{m,0}$ and $\sigma_{b,0}$ being calculated for the

Table 2
Coefficients C in Eqns. (14)–(16).

Point at crack front	C_{10} [−]	C_{11} [−]	C_{20} [−]	C_{21} [−]
A	0.0167	−1.8496	−1.5310	3.5736
C	0.0113	−0.4266	−0.9405	2.8513

Table 3
Coefficients C in Eqn. (17).

Point at crack front	C_0 [−]	C_1 [−]
A	1.4374	−1.2067
C	1.5966	−0.6823

critical crack size obtained in step 5 under the proportional loading assumption (i.e. $\sigma_b^* = \gamma \cdot \sigma_m^*$).

Note that in real applications the bending stress component could be negative (i.e. the bending stress component would have the effect of closing the crack). In such a case the correction factor $\sigma_m^*/\sigma_{m,0}$ would become larger than 1 if the formal correction is used and the critical stress obtained in step 5 would be increased and not reduced. Within the procedure proposed here this is, however, not permitted to ensure conservatism of the final analysis results. Therefore the correction factor which takes into account the bending stress component is given as

$$\alpha = \frac{\text{critical load}_{\text{final}}}{\text{critical load}_{\text{step 5}}} = \min\begin{cases} \sigma_m^*/\sigma_{m,0} \\ 1 \end{cases} \tag{22}$$

3. Validation

3.1. Burst tests

Four burst tests[1] have been conducted on thick-walled pipe pieces such as those used in hydraulic cylinders for earthmoving machinery. The tests have been performed in order to determine the critical conditions, i.e., values of the pressure at burst and failure mode. The components were pipes with nominal outer diameter $D_o = 155$ mm and nominal wall thickness $T = 15$ mm. The length of the tube pieces was $l = 400$ mm. Longitudinal artificial defects were machined onto the outer surface of the pipes by EDM; the initial artificial defects had a rectangular shape described by an aspect ratio $a/c = 0.2$ and normalized depth $a/T = 0.05$ (see the fracture surface on top left of Fig. 4). Subsequently the pipes with the initial artificial defects have been mounted on a special testing facility [19], and have been fatigue pre-cracked using pulsating internal pressure (i.e. cyclic loading). A thermocouple has been glued to the pipes and connected to a control panel in order to check the temperature rise during fatigue pre-cracking. The crack depth has been controlled and monitored using a measurement device based on the potential drop method. The machined rectangular defects, during fatigue pre-cracking, developed into semi-elliptical cracks with crack depth a_0 and crack length $2c_0$ (see the fracture surface on top left of Fig. 4). The semi-elliptical crack dimensions at the end of the pre-cracking stage are reported in Table 4.

After the fatigue pre-cracking stage, the pipes have been equipped with caps, which have been welded at the free ends of the pipes. The burst tests were then carried out on capped-end pipes at a temperature of −20 °C, which represents the lowest in-service temperature for the pipes. Alcohol was used to fill up the capped-end pipes, and aluminum filler bars have been used to avoid excessive pressurized volume. The tests have been conducted on a different test device for security reasons; a thermocouple wire has been used for temperature control purpose. It is important to remark that during the burst test the potential drop device has not been used, therefore it has been not possible to monitor the stable crack advance with increasing pressure.

[1] The tests have been performed at Tenaris Dalmine.

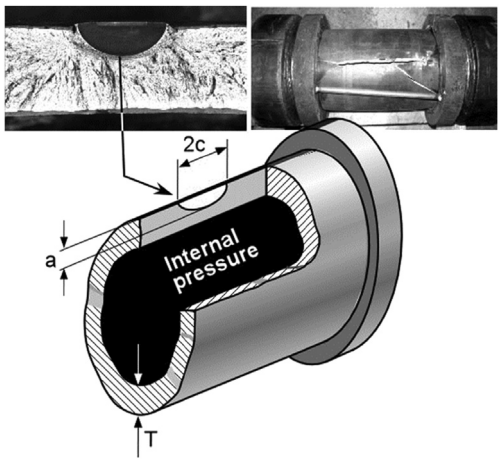

Fig. 4. Top: Fracture surface of Pipe #2 after the burst test. Bottom: Schematic drawing of the capped-end pipes.

The internal pressures at failure and the corresponding critical crack dimensions at the deepest point of the semi-elliptical crack have been obtained as given in Table 5. Note that the fractographic determination of the critical crack length at surface $2c_c$ faced with some uncertainty due to irregularity of the final crack front near its surface points. Therefore this information will not be used for validation.

For all tested pipes, failure occurred as burst and not by a leak before break (LBB) scenario. The fractographic analyses showed the ductile tearing phases terminated by unstable longitudinal crack extension. Fig. 4, on the top, shows the fracture surface of Pipe #2 after the burst test, while a schematic drawing of a capped-end pipe with a semi-elliptical axial surface crack on the outer surface is given at the bottom.

3.2. Analytical determination of the stress profiles in the component

The elastic stresses for the unflawed thick-walled pipes subjected to internal pressure p_i, were obtained using Lame's formulation [20]. The principal stresses for closed-end conditions can be expressed as:

Table 4
The crack dimensions after the fatigue pre-cracking stage.

	Crack depth a_0 [mm]	Crack length $2c_0$ [mm]
Pipe #1	13.5	33.0
Pipe #2	5.8	15.0
Pipe #3	8.0	17.5
Pipe #4	9.4	23.0

Table 5
Burst tests results ($D_o = 155$ mm and $T = 15$ mm).

	Critical pressure p_c [MPa]	Critical crack depth a_c [mm]
Pipe #1	138	14.2
Pipe #2	165	7.0
Pipe #3	159	8.5
Pipe #4	151	10.3

$$\sigma_r = \frac{p_i}{k^2-1}\cdot\left(1-\frac{r_o^2}{r^2}\right)$$
$$\sigma_\theta = \frac{p_i}{k^2-1}\cdot\left(1+\frac{r_o^2}{r^2}\right) \quad (23)$$
$$\sigma_a = \frac{p_i}{k^2-1}$$

where $k = r_o/r_i$.

Note that the hoop stress σ_θ is the stress perpendicular to the crack plane. Therefore it has been employed in the calculation of the stress intensity factors and the main loading component in the calculation of the reference yield stress, whereas σ_a is the stress parallel to the crack plane, thus defining the biaxiality stress ratio in Eqn. (6) as $\lambda = \sigma_a/\sigma_\theta$.

3.3. Material properties

The material used is a high strength, high toughness steel, with the following basic mechanical properties at −20 °C: $\sigma_Y = 655$ MPa, $R_m = 760$ MPa. The true stress–strain curve at −20 °C is depicted in Fig. 5, in which the true stresses have been normalized by the yield strength σ_Y. Even though all components were manufactured as seamless tubes, no evidence of anisotropy was found upon experimental testing.

The crack resistance R-curve can be obtained by standard test procedures [6,21,22] on deeply notched SE(B) or C(T) specimens which show a high crack tip constraint and will hence provide lower bound estimates for the fracture resistance. However pressurized piping systems are used to be characterized by a reduced crack tip constraint as compared to standard specimens. Therefore, recent defect assessment procedures allow the use of test specimens which more closely match the crack tip constraint in the structural component [4].

A number of studies have supported the use of single edge notched tension specimens SE(T) for experimental R-curves relevant to piping systems [23–26], in order to reduce the potential conservatism. However, despite a substantial volume of literature supporting the use of SE(T) specimens in fracture toughness testing for pipe application, no standard test methods are yet available, see, however, the developments in Ref. [27]. In the present study, the recommended practice of DNV [23] has been used for the design of the SE(T) specimens (Fig. 6). The dimensions were: width $W = 12.8$ mm, thickness $B = 14$ mm and distance between grips $H = 142$ mm. The specimens were machined with an initial notch of 3 mm depth, and then fatigue pre-cracked using a three-point bend apparatus. Subsequently, the specimens were side-grooved to a net thickness $B_N = 0.8\cdot B$ (10% side-groove on each side) in order to generate plane strain conditions along the crack front and to promote uniform crack growth.

The specimens were tested at the same temperature as applied to the burst tests, i.e. at −20 °C. For each test a load versus crack mouth opening displacement (CMOD) record was obtained. The DNV fracture resistance testing procedure is based on the multiple specimen technique and no guidance is provided on the use of single specimen techniques. However, in the present study, single specimen technique had to be used due to the scarce availability of specimens. Particularly, the key-curve method has been used to estimate crack extension from the load-CMOD curves.

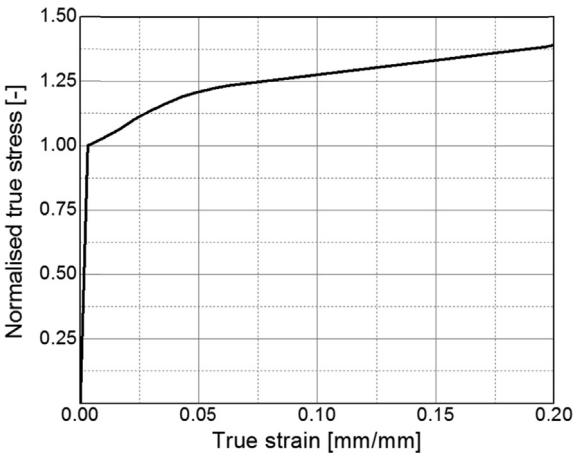

Fig. 5. Normalized true stress–strain curve of the material tested at −20 °C.

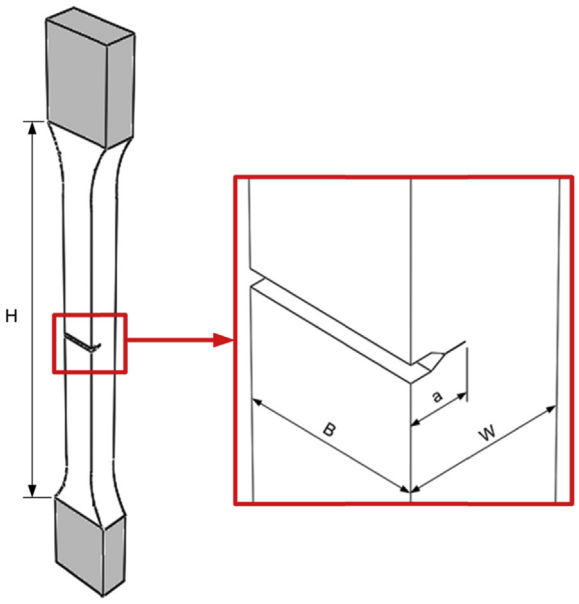

Fig. 6. Clamped SE(T) specimen configuration.

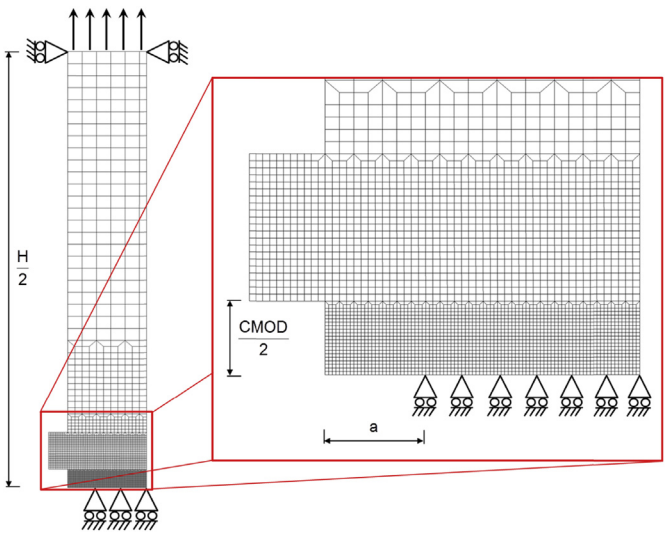

Fig. 7. Plane strain model employed in the finite element calculations.

The key-curve method was developed by Ernst [28,29] as a method for the determination of R-curves from single load–displacement curves without the use of additional crack length measurement techniques. Fig. 8 illustrates its numerical option. FEM based Load-CMOD curves are obtained from multiple nonlinear finite element analyses for the test specimen configuration with stationary cracks of different depths. These curves are then plotted in one diagram together with the experimental load-CMOD curve of a real test specimen. In the real specimen crack extension occurs, because of which the intersections between the experimental curve and the (stationary) numerical curves can be used to estimate the crack extension in the experimental diagram. Plane strain numerical key-curves were obtained and successfully tested against experimental results for a large range of steels with different strengths and toughness in Ref. [30], and a more recent example for HY80 steel, the yield strength of which (630 MPa) is comparable to the material investigated in this study, is presented in Ref. [31].

Since no key-curve solutions were available for SE(T) specimens, these had to be determined within the present study. Nonlinear finite element analyses were performed on plane strain models of the SE(T) specimen geometry (see Fig. 7). The use of plane strain finite element analyses is strongly supported by the similarity between the 2D and 3D finite element analyses of SE(T) fracture specimens reported in Refs. [25,32–34]. The model consists of 3328 plane strain elements with 8 nodes and reduced integration. The structured mesh has been highly refined approaching the ligament (see magnification in Fig. 7) to the aim of having a well-defined and smooth description of the specimen compliance as a function of the crack advance Δa. In particular, the element size along the ligament has been set to 0.15 mm. It has been taken advantage of the symmetry conditions, therefore just half of the specimen has been modeled. Furthermore the clamped boundary condition given by the grips of the machine has been realized by constraining the displacements perpendicular to the specimen axis on the top edge of the model. On the same edge a progressive traction has been applied for simulating the external loading. The values of the CMOD have been recorded at one node set at the same position of the tip point of the clip-on gage in the experimental tests (see magnification in Fig. 7). The material behavior has been modeled according to the true stress–strain curve depicted in Fig. 5.

The application of the method to one of the test specimens is shown in Fig. 8, whereas the R-curves derived from all three specimens are depicted in Fig. 9. It is of some importance to underline the good repeatability offered by the method, as all the curves lie in a quite narrow scatter band.

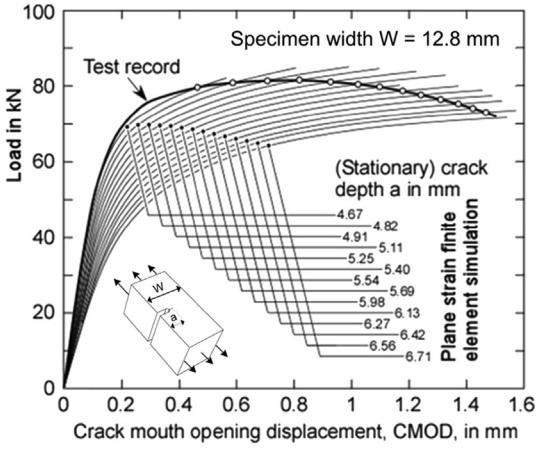

Fig. 8. Determination of the crack length during test from the load-CMOD curve by a finite element based key-curves.

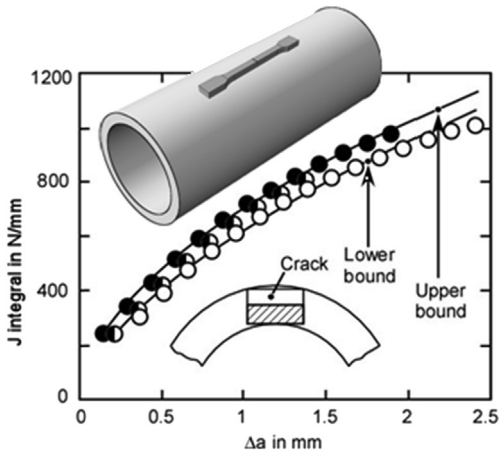

Fig. 9. $J-\Delta a$ crack resistance (R-curves) obtained by the key-curve method on 3 SE(T) specimens.

For the sake of clarity and comparison, only the lower bound (LB) and upper bound (UB) R-curves are considered in the assessment procedure in the following. Their analytical formulation is given as follows:

$$J = \begin{cases} 624 \cdot \Delta a^{0.61} & \text{lower bound} \\ 701 \cdot \Delta a^{0.54} & \text{upper bound} \end{cases} \tag{24}$$

Both curves refer to one of the three tested specimens, this way indicating the scatter band in the R-curve.

Furthermore, in order to verify the accuracy of the method, it has been important to compare the optically measured crack extension $\Delta a_{measured}$ at the end of the tests with the value predicted by the method, $\Delta a_{predicted}$. According to the standards, the crack extension has been provided as the average of 9 equally spaced measurements along the crack front upon fracture. Table 6 provides the measured and predicted crack extension, as well as the absolute percentage error for all the tested specimens.

3.4. Comparison between experiments and predictions: results and discussion

The proposed assessment methodology has been applied to predict the instability loads of the burst tests. Fig. 10 shows the result obtained for Pipe #2. The lower bound R-curve has been used, and the biaxial stress ratio was assumed to be $\lambda = 0.5$ which is typical for pressurized piping components.

However, the prediction revealed the initial ductile stable tearing phase terminated by failure due to plastic collapse prior to tearing instability. In the figure only the analysis for the surface points is shown since this, compared to the deepest point at the crack front, yielded the lower critical loads. This result agrees with

Table 6
Optically measured and predicted crack extensions (values provided in mm).

Specimen	Optical measurement			Key-curve method			|Error| [%]
	a_0	a_f	Δa	a_0	a_f	Δa	
SE(T)#1	4.67	6.70	2.03	4.67	6.56	1.89	7
SE(T)#2	4.74	7.30	2.56	4.74	7.15	2.41	6
SE(T)#3	4.75	6.15	1.40	4.75	6.13	1.38	1

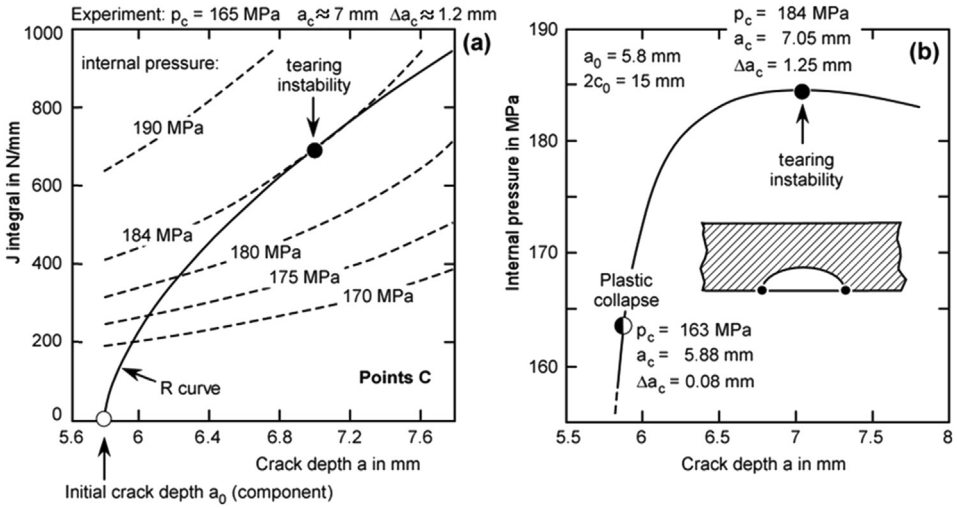

Fig. 10. Application of the proposed method to the burst test of Pipe #2. The lower bound R-curve has been used. However, it showed up that the failure would occur by plastic collapse prior to tearing instability.

the fractographic evidences reported in Fig. 4, which clearly show the fracture starting from sub-surface points along the crack front.

Fig. 11 provides a comparison between the experimental and the predicted critical pressures. Note that for all tests the critical con-dition was reached first at the surface points of the cracks. As a result it can be concluded that the leak-before-break criterion is not fulfilled which is in accordance with the experimental observations. The predicted critical pressures were conservative within the 5% tolerance band (see also Fig. 12). The only point which was outside of this tolerance band was the burst test of Pipe #1 characterized by $a_0/T = 0.92$, for which no valid analytical solution of the *K*-factor and reference yield stress were available. Nevertheless, even this prediction was conservative. Note however, that the solutions should not be used outside their validity range or, if this is the case, the results must be analyzed carefully. The predicted and experimental critical internal pressures are given in Table 7.

The critical pressure values obtained by the proposed methodology have been compared with predictions according to solutions available in the literature. Peculiarly suited in this case is the local limit pressure solution for thick-walled cylinders with axial surface cracks proposed by Lei [10]. The comparison has been carried out using the lower bound curve in Eqn. (24) and it is provided in Fig. 12. The proposed method allowed the achievement of a reduced conservatism, which, according to the authors, is mainly due to a better description of the dependence of the crack driving force on applied pressure given by the new reference yield stress solutions which account for biaxiality.

4. Summary and conclusions

In the present paper, a methodology for fracture instability analysis is developed which combines both, biaxial and combined tension-bending loading. The analyses have been carried out analytically using a reference yield stress solution previously proposed by the authors.

Fracture resistance testing employed side-grooved, clamped SE(T) specimens ($a/W = 0.37$). The key-curve method has been used for obtaining R-curves with a single specimen technique, showing a very consistent prediction of stable crack growth compared to the test records.

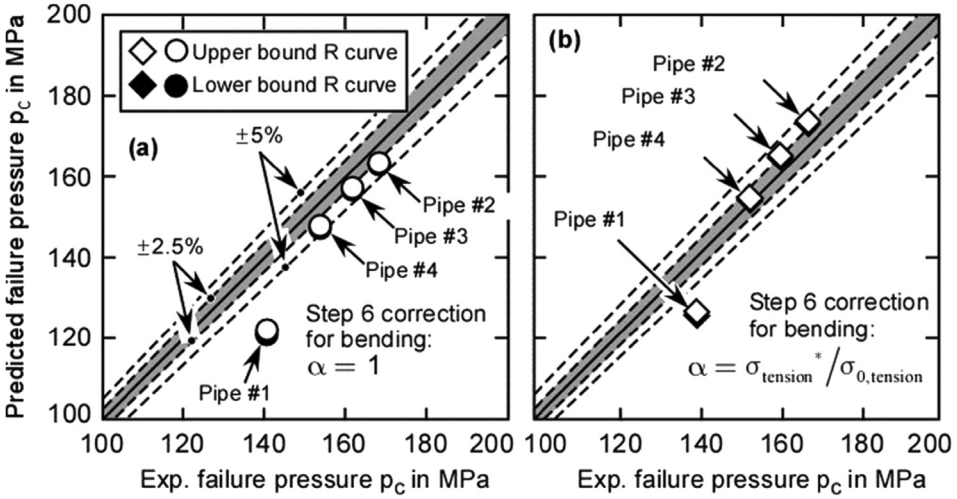

Fig. 11. Comparison between the experimental and predicted failure pressures of the four burst tests: a) with the correction factor for bending $\alpha = 1$ (as recommended); b) with the correction factor for bending $\alpha = \sigma_m^*/\sigma_{m,0}$ (see Fig. 5).

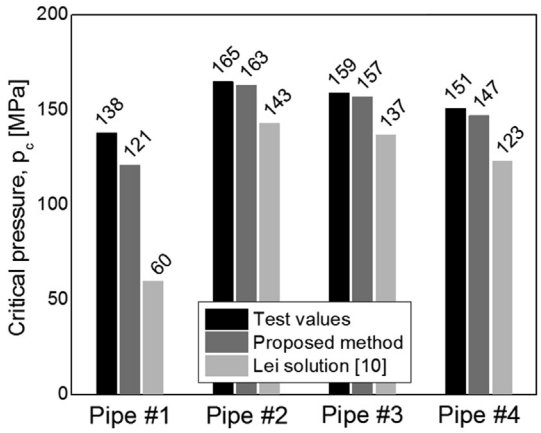

Fig. 12. Critical pressures (p_c in MPa) as predicted using the lower-bound R-curve by the proposed approach and using the local limit pressure solution by Lei [10] in comparison with the experimental evidences (Note that some of the analytical solutions have been used outside their validity range in case of Pipe #1).

Table 7
Predicted and experimental critical pressures (p_c in MPa) of the four burst tests.

	Predicted lower bound critical pressure[a]	Predicted upper bound critical pressure[b]	Experimental critical pressure
Pipe #1	121	122	138
Pipe #2	163	164	165
Pipe #3	157	157	159
Pipe #4	147	148	151

[a] Lower bound R-curve.
[b] Upper bound R-curve.

The proposed assessment methodology has been validated by burst tests conducted on thick-wall pressurized pipes containing artificial semi-elliptical axial flaws onto the external surface. The comparison of the predicted and test failure pressures showed satisfying agreement. The only exception was the deeply cracked pipe with ($a_0/T = 0.92$) for which the experimental value has been underestimated by 12%. Note however that the corresponding crack dimensions of this case were substantially beyond the validity ranges of both the *K*-factor and reference stress solutions used in this study.

Moreover the proposed method, based on reference yield stress solutions for biaxial loading, showed a reduced conservatism compared to a standard instability analysis based on well-established solutions.

Acknowledgments

Diya Arafah would like to acknowledge the Federal Institute for Materials Research and Testing (BAM), in particular the leader of the Department 9, Prof. Thomas Böllinghaus, and the leader of the Division 9.1, Prof. Dietmar Klingbeil, for providing him support during his stay in Germany as visiting PhD student.

Dr. Mario Rossi, director of Tenaris Dalmine Research & Development Center, is kindly acknowledged for permission to publish this work.

Appendix. Brief outline of the reference yield stress method

In Refs. [12–14] two of the authors of the present paper suggested to replace the yield or limit load by a reference load F_0 which they basically obtain by finite element analyses. It is defined as that load at which the condition

$$\frac{J}{K^2/E} = \frac{J}{J_e} = [f(L_r = 1)]^{-2} \tag{A1}$$

is satisfied. The $f(L_r)$ value for $L_r = 1$ is obtained from the Option 2 of R6 by

$$f(L_r) = \left[\frac{E \cdot \varepsilon_{ref}}{\sigma_{ref}} + \frac{1}{2} \cdot \frac{\sigma_{ref}}{E \cdot \varepsilon_{ref}} \cdot L_r^2\right]^{-1/2} \tag{A2}$$

with $L_r = 1, \sigma_{ref} = R_{p0.2}$ and $\varepsilon_{ref} = R_{p0.2}/E + 0.002$. The principle is illustrated in Fig. A1. It can be applied on the basis of forces and moments (Fig. A1a) but also on the basis of stresses (Fig. A1b). In the latter case the parameter is designated as reference yield stress σ_0.

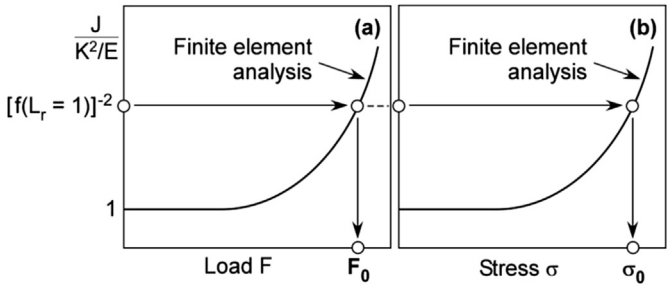

Fig. A1. Principle of the determination of (a) the reference load F_0 and (b) the reference yield stress σ_0.

Note that F_0 (and σ_0) by its nature, is not a limit load. Instead of referring to the whole ligament it is, although an applied load, a local parameter. Therefore, different F_0 or σ_0 values are obtained for the deepest and surface points of the semi-elliptical surface cracks. It is possible not only to generate very accurate solutions for the use in R6 or similar methods, but also offers the possibility to generate parameter solutions, see Refs. [12,13] (and the present study). These solutions can be used without the need of individual finite element analyses.

Note that the reference load approach is close to the original methodology of the R6-like concepts. Historically, the use of limit loads instead of a reference loads occurred at a later time for pragmatic reasons since such solutions were simply available and could be summarized in compendia, and because it was shown for a number of standard geometries that their values were slightly conservative compared to the reference loads (see the discussion in Ref. [14]). The advantage of the use of limit instead of reference loads was that the R6 method immediately could be applied to a large number of geometries (which was responsible for its success) but the price was reduced accuracy. The reference load method used in the present paper goes back to the roots but provides solutions the use of which is as convenient as the use of the limit load solutions. The improved accuracy has been demonstrated in earlier papers of the authors [12,13].

References

[1] Papadakis GA. Major hazard pipelines: a comparative study of onshore transmission accidents. J Loss Prev Process Ind 1999;12:91–107.
[2] Doglione R, Firrao D. Structural collapse calculations of old pipelines. Int J Fatigue 1998;20:161–8.
[3] Choi JB, Goo BK, Kim JC, Kim YJ, Kim WS. Development of limit load solutions for corroded gas pipelines. Int J Press Vessels Pip 2003;80(2):121–8.
[4] R6, Revision 4. Assessment of the integrity of structures containing defects. Gloucester, UK: EDF Energy Nuclear Generation Ltd.; 2013.
[5] Zerbst U, Schödel M, Webster S, Ainsworth RA. Fitness-for-service fracture assessment of structures containing cracks. A workbook based on the European SINTAP/FITNET procedure. Elsevier; 2007.

[6] American Society for Testing and Materials. Standard test method for linear-elastic plane-strain fracture toughness K_{Ic} of metallic materials. 2011. ASTM E399-11.
[7] API 579-1/ASME FFS-1. Fitness-for-service. American Petroleum Institute and American Society of Mechanical Engineers; 2007.
[8] BS 7910. Guides on methods for assessing the acceptability of flaws in metallic structures. British Standard Institution (BSI); 2005.
[9] Staat M, Vu DK. Limit analysis of flaws in pressurized pipes and cylindrical vessels. Part I: axial defects. Eng Fract Mech 2007;74(3):431–50.
[10] Lei Y. A review of limit load solutions for cylinders with axial cracks and development of new solutions. Int J Press Vessels Pip 2008;85(12): 825–50.
[11] Kim Y-J, Shim D-J. Relevance of plastic limit loads to reference stress approach for surface cracked cylinder problems. Int J Press Vessels Pip 2005;82(9): 687–99.
[12] Zerbst U, Kiyak Y, Madia M, Burgold A, Riedel G. Reference loads for plates with semi-elliptical surface cracks subjected to tension and bending for application within R6 type flaw assessment. Eng Fract Mech 2013;99:132–40.
[13] Madia M, Arafah D, Zerbst U. Reference load solutions for plates with semi-elliptical surface cracks subjected to biaxial tension loading. Int J Press Vessels Pip 2014;119:19–28.
[14] Zerbst U, Ainsworth RA, Madia M. Reference load versus limit load in engineering flaw assessment: a proposal for a hybrid analysis option. Eng Fract Mech 2012;91:62–72.
[15] Arafah D, Madia M, Beretta S, Cristea M. Structural integrity assessment of thick wall pipes under biaxial loading. In: Proceedings of 19th European Conference on Fracture (ECF19), 26–31 August 2012. Russia: Kazan; 2012.
[16] Arafah D. Fracture assessment of cracked components under biaxial loading. Politecnico di Milano; 2014. PhD Thesis.
[17] Murakami Y, Hasebe MT, Itoh Y, Kishimoto K, Miyata H, Miyazaki N, et al., editors. Stress intensity factors handbook, vol. 1 and 2; 1987-2001. Vol. 3: 1992, Vol. 4 and 5: 2001.
[18] Raju I, Newman J. Stress-intensity factors for internal and external surface cracks in cylindrical vessels. J Press Vessel Technol 1982;104(4):293–8.
[19] Cristea M, Beretta S. Structural integrity assessment validation of seamless tubes for hydraulic cylinders using fitness for service concepts. In: Berger C, Schwalbe KH, editors. Proceedings of ECF 18; 2010. p. 1–10.
[20] Budynas RG. Advanced strength and applied stress analysis. 2nd ed. New York: McGraw-Hill; 1999.
[21] American Society for Testing and Materials. Standard test method for measurement of fracture toughness. 2009. ASTM E1820-09.
[22] International Standard. Metallic materials – unified method of test for the determination of quasi-static fracture toughness. 2002. ISO 12135.
[23] Det Norske Veritas. Fracture control for pipeline installation methods introducing cyclic plastic strain. 2006. DNV-RP-F108.
[24] Cravero S, Ruggieri C. Estimation procedure of J-resistance curves for SE(T) fracture specimens using unloading compliance. Eng Fract Mech 2007;74(17): 2735–57.
[25] Mathias L, Sarzosa D, Ruggieri C. Effects of specimen geometry and loading mode on crack growth resistance curves of a high-strength pipeline girth weld. Int J Press Vessels Pip November–December 2013;111–112:106–19.
[26] Shen G, Tyson WR. Crack size evaluation using unloading compliance in single-specimen single-edge notched tension fracture toughness testing. J Test Eval 2009;37(4). JTE102368.
[27] Pisarski H, Moore Ph, Hutchison E. Development of a British Standard single edge notch tension (SENT) test method (BS 8571). In: 6th International Pipeline Technology Conference (Rudi's Pipeline Conference), 6–9 October 2013. Belgium: Ostend; 2013.
[28] Ernst H, Paris PC, Rossow M, Hutchinson JW. Analysis of load-displacement relationship to determine J-R-curve and tearing instability material properties. 1979. p. 581–99. ASTM STP 667.
[29] Joyce JA, Ernst HA, Paris PC. Direct evaluation of J-Resistance curves from load displacement record. 1980. p. 222–36. ASM STP 700.
[30] Brüninmghaus K, Falk J, Twickler M, Dahl W. Determination of crack resistance curves under static and dynamic loading by analysis of load displacement relationship. Eng Fract Mech 1989;34:898–1000.
[31] Qian X, Yang W. A hybrid approach to determine ductile fracture resistance. Proc Eng 2011;10:319–24.
[32] Cravero S, Ruggieri C. Correlation of fracture behavior in high pressure pipelines with axial flaws using constraint designed test specimens–part I: plane-strain analyses. Eng Fract Mech 2005;72(9):1344–60.
[33] Silva LA, Cravero S, Ruggieri C. Correlation of fracture behavior in high pressure pipelines with axial flaws using constraint designed test specimens. Part II: 3-D effects on constraint. Eng Fract Mech 2006;73(15):2123–38.
[34] Ruggieri C. Further results in J and CTOD estimation procedures for SE(T) fracture specimens – part I: homogeneous materials. Eng Fract Mech 2012;79:245–65.